Polymer Degradation and Stability 195 (2022) 109805

Thermal response of multi-layer UV crosslinked PEGDA hydrogels

Mohammad Hakim Khalili[1], Ashfaq Afsar[2], Rujing Zhang[3], Sandra Wilson[3], Eleftheria Dossi[2], Saurav Goel[4,5,6], Susan. A Impey[1], and Adrianus Indrat Aria[1] *

Affiliation:

1. Surface Engineering and Precision Centre, School of Aerospace, Transport and Manufacturing, Cranfield University, MK430AL, United Kingdom
2. Centre for Defence Chemistry, Cranfield University, Shrivenham, Swindon, SN6 8LA
3. Sophion Bioscience A/S, Baltorpvej 154 2750 Ballerup, Denmark
4. London South Bank University, 103 Borough Road, London, SE1 0AA, United Kingdom
5. Indian Institute of Technology Guwahati, Guwahati, 781039, India
6. University of Petroleum and Energy Studies, Dehradun, 248007, India

*** Corresponding author: a.i.aria@cranfield.ac.uk; ORCID: 0000-0002-6305-3906**

Abstract

Poly(ethylene glycol) diacrylate (PEGDA) hydrogels are ubiquitously used in a wide variety of applications in tissue engineering. In this study, the thermal response of multi-layered PEGDA hydrogels was investigated under various conditions of the temperature-controlled environments (8, 20, 37, and 45 °C) through gravimetric and volumetric methods. These multi-layered hydrogels were produced using a computer-controlled projection lithography and compared to the monolithic hydrogels fabricated through bulk photo-crosslinking. It was observed that the volume of multi-layered PEGDA hydrogels increased to about 10% at a temperature of 8 °C, while their volume decreased by 8% and 12% when stored at 37 °C and 45 °C, respectively. PEGDA hydrogel also showed an anisotropic characteristic where the axial dimensional change was about 43% higher than the lateral dimension. This finding is critical to inform the design and fabrication of PEGDA hydrogels to compensate for the axial and lateral volume changes during the application at different temperatures.

Keywords:

poly (ethylene glycol) diacrylate, projection lithography, thermoresponsive hydrogel, multi-layered structures

1. Introduction

Rapid advances in biomedical engineering are underpinned by the development of smart functional materials that exhibit excellent biocompatibility and tunable mechanochemical properties [1–5]. The mechanical properties of hydrogel can be precisely controlled to mimic a desired tissue microenvironment for use as tissue scaffolds with behaviour similar to that of an extracellular matrix [6–9]. Their physicochemical properties, such as compactness and low interfacial tension with aqueous media, resemble living tissues due to their high affinity to water [10–12]. These properties have allowed hydrogels to be widely used in many biomedical applications including drug delivery and tissue engineering [13,14].

The emergence of poly (ethylene glycol) diacrylate (PEGDA) as candidates for biomaterials can be attributed to their approved low-immunogenic biocompatibility and ability to be photo-crosslinked using appropriate photoinitiator [15,16]. With the recent development in lithographic additive manufacturing [17,18], the multi-length scale structure and morphology of PEGDA can be tailored to exhibit unique bio-functionality of complex 3D scaffolds [19]. In addition, the biomechanical properties of PEGDA can be tuned by controlling the molecular weight, light irradiation dosage, and concentration of photoinitiator and photoabsorber during the crosslinking process [20,21].

To date, the fundamental understanding of the long-term thermomechanical behaviour of PEGDA has not been established [22–24]. The aim of this study was to elucidate the effect of external temperature on the long-term dimensional stability of photo-crosslinked PEGDA

to address their thermal response in various environmental conditions that differ to the fabrication conditions. We report herein that the equilibrium volume of PEGDA hydrogels increases by ~10% when they are in the cold storage temperature of 8°C and decreases by ~8% when they are in the body temperature of 37°C. We also demonstrate that their thermal response is fully reversible, which expand the possibility of mass production and scale-up use of photo-crosslinked PEGDA hydrogels. Our approach and analysis offer insights into long term stability of hydrogels that can be extrapolated further to other biomaterials for the benefit of many biomedical engineering applications.

2. Materials and methods

2.1 Synthesis of PEGDA 3D structures

The starting material for the aqueous prepolymer solution contained 5 mg/mL Lithium phenyl-2,4,6-trimethylbenzoylphosphinate photoinitiator (LAP; Merck 900889, ≥ 95%) and 200 mg/mL Poly (ethylene glycol) diacrylate (PEGDA; Merck 455008, Mn 700 g/mol). Multi-layered PEGDA hydrogel samples were created by projecting an image of a photomask (10k resolution from Photo Data) using a custom-made computer-controlled projection lithography. The system uses a projection of a static image, attached at the bottom of the vat, to construct a layer-by-layer structure until the required height is reached (Figure 2a). Layer thickness was set at nominal thickness of 20 µm and 150 µm and the manufactured hydrogel structures are denoted herein as multi-20 µm and multi-150 µm, respectively. For fabrication of multi-20 µm and multi-150 µm, 9 and 1.8 mg/mL Quinoline Yellow photoabsorber (QY; Merck 309052) was also added to the prepolymer solutions,

respectively [17]. The presence of the QY photoabsorber in the prepolymer solution made the colour of the crosslinked sample yellow (Figure 2a,b). Each layer was exposed for 3 s to the UV light with wavelength of 365 nm at an intensity of 20 mW/cm^2, equivalent to 120 mJ/cm^2 dosage, as each layer was exposed twice (Figure 2d,e). The structure was fabricated on the surface of a treated coverslip glass (24 x 24 x 1 mm. Agar Scientific AGL4367). The coverglasses were washed in three baths inside a sonication device (10 mins in each bath): 1. DI water and soap, 2. acetone and 3. isopropanol. They were then dried using an air blower. After that, they were transferred to an oxygen plasma chamber (Diener Atto) for 3 cycles of 2.5 mins at the power of 50 W to remove any organic contaminants. Then, they were placed in a bath of solution mix of 2%v/v of 3-(trimethoxysilyl) propyl methacrylate (TMSPMA; Merck 440159) in 94-96% ethanol for 10 mins, washed with ethanol 99% for 3 times, and then placed on a hot plate set at 110 °C for another 10 mins to dry them off [21]. The treatment created a methacrylate layer on the surface of the coverglass to allow covalent binding with the fabricated hydrogels [25].

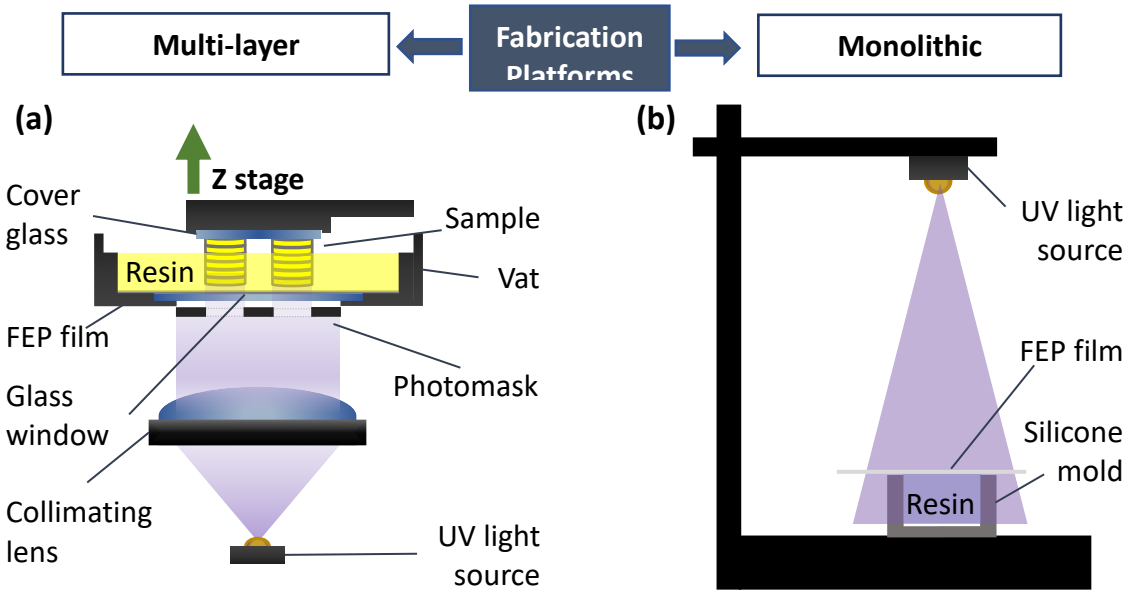

Figure 1: Schematic of fabrication platforms of **(a)** computer-controlled projection lithography for multi-layered hydrogel structures and **(b)** fixed-photo-crosslinking setup for monolithic hydrogel structures.

As control samples, monolithic structures were created in a 10 x 10 x 5 mm silicone mould using single exposure bulk crosslinking with 0.5 mL of PEGDA and LAP mix solution without QY. A thin layer of Fluorinated Ethylene Propylene (FEP) was placed on top of the mould to remove excess solution and to flatten the shape of the intended cuboid (Figure. 1b). The solution was exposed to 3 s of UV light at 40 mW/cm^2 to equate to the same dosage as for every layer of the multi-layered structure that was 120 mJ/cm^2 (Figure. 2c). The fabricated monolithic hydrogel structures are denoted herein as mono-5 mm. The fracture like interfaces in the monolithic samples were from the surface of silicone mould that the samples were crosslinked in (Figure. 2f). Two additional types of monolithic samples were fabricated with structure height of 1.5 mm and 3 mm., which are denoted herein as mono-

1.5 mm and mono-3 mm. Those samples were used to examine the effect of the overall hydrogel structures' height on the thermal response of the hydrogel.

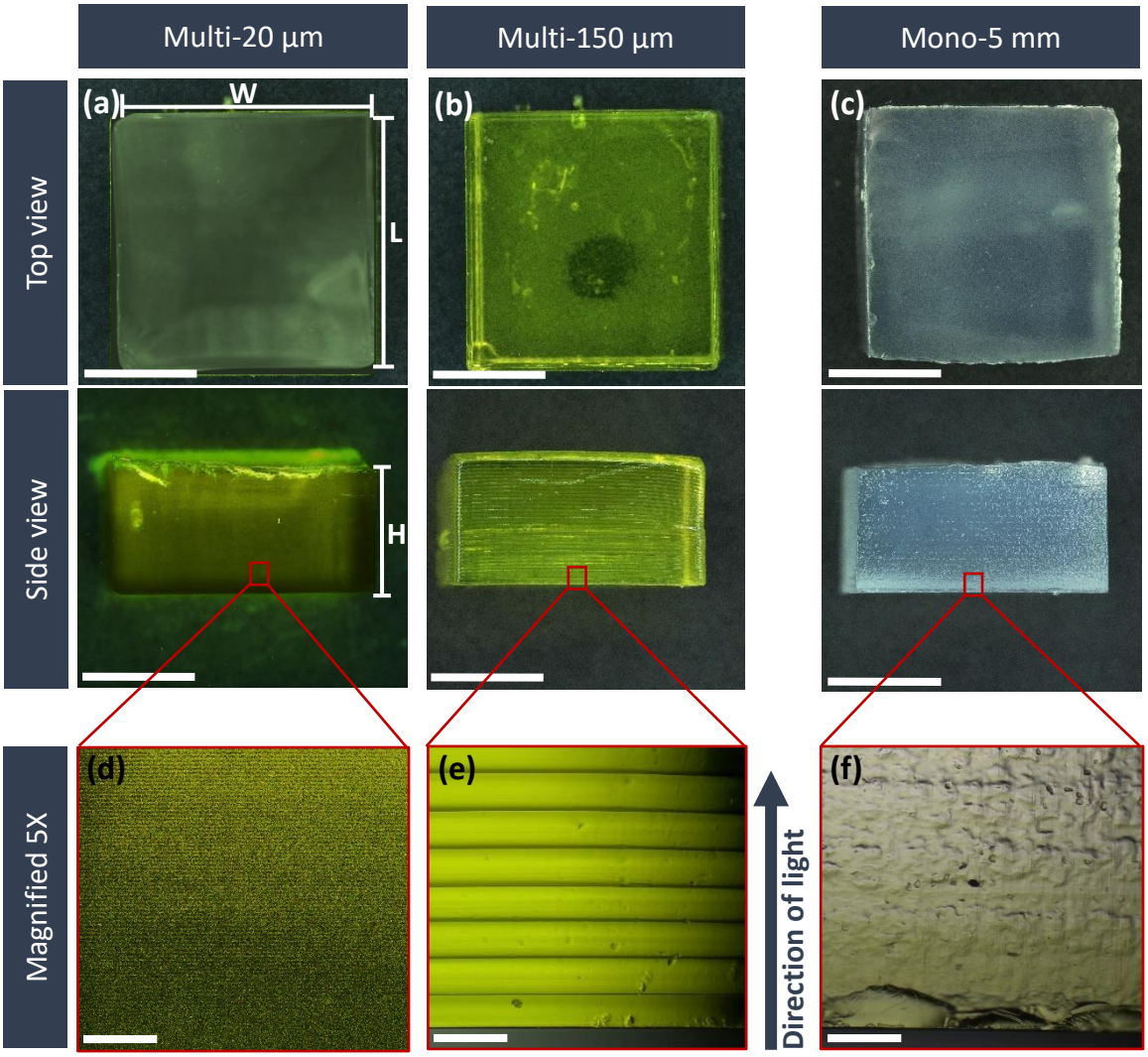

Figure 2: Top and side view photographs of multi- **(a)** 20 µm and **(b)** 150 µm and **(c)** mono-5 mm PEGDA hydrogels. Side view microscopy images of multi- **(d)** 20 µm and **(e)** 150 µm and **(f)** mono- 5mm PEGDA hydrogels. Scale bars in (a), (b) and (c) are 5 mm and in (d), (e) and (f) are 300 µm.

2.2 1H NMR measurements

All starting materials and the residual fraction from storage of selected multi-20 μm and multi-150 μm and mono-5 mm PEGDA hydrogels were characterised with Proton Nuclear Magnetic Resonance (^{1}H NMR) spectroscopy (Bruker Ascend 400 MHz spectrometer) with a BBFO probe, at an ambient temperature. The solvent peaks were referenced to 4.7 ppm (HDO, D_2O) using Tetramethylsilane (TMS; Merck 87920, ≥99.5%, Mn 88.22 g/mol) as an internal standard. Hydrogel samples were stored in 7 mL of DI water immediately after fabrication, for 24 hrs, allowing time for the unreacted polymer to leach out of the hydrogel structure. The DI water solution was then dried under vacuum to get rid of all moisture. The remaining solid residue was dissolved in 1 mL of Deuterium oxide (D_2O; Merck 151882, ≥99.9%, Mn 20.03 g/mol) and was characterised by ^{1}H NMR. The glass transition temperature of the PEGDA hydrogels was determined by Differential Scanning Calorimetry (DSC; Mettler Toledo, DSC 3+ STAR System).

2.3 Gravimetric and volumetric measurements

PEGDA hydrogels thermal response was investigated through gravimetric and volumetric methods. Samples were transferred to individual temperature-controlled water baths at 8, 20, 37 and 45 °C inside a fridge or environmental cabinet. Temperatures 8 and 45 °C were chosen to represent cold-storage and transportation temperatures, 20 °C is the fabrication temperature, and 37 °C was the incubation temperature mimicking the biomedical application environment. For each temperature, 4 samples of multi-20 μm and multi-150

µm cuboid PEGDA hydrogels with dimensions 5 x 5 x 10.05 mm and 4 samples of mono- 5 mm cuboids with dimensions 10 x 10 x 5.1 mm were fabricated.

All hydrogel samples were weighed immediately after fabrication and placed in their designated water bath. At predetermined time points, every 1.5-2 hrs for 6 hrs and every 24 hrs for 168 hrs, the hydrogel samples were removed from their water baths, gently blotted using medical wipes (Kimberly Clark) and weighed. The samples were then dried at the end of the 168 hrs of the study using freeze-drying. The hydrogels were removed from their water baths and put straight inside a liquid nitrogen bath for 60 s. They were then transferred to a freezer set at -20 °C until all samples were frozen using liquid nitrogen. All samples were transferred into freeze dryer (Christ Alpha 1-2 LD plus) with condenser temperature and sublimation pressure set at -60 °C and $1.1x10^{-2}$ mbar and kept overnight. Their dried weight (M_d) was measured the following day using an analytical balance (Ohaus AS60C) with repeatability of ±0.1 mg.

The Normalised Weight Fraction (NWF) was calculated using the equation

$$NWF = M_s/M_0 \qquad \text{(Eq. 1)}$$

Where (M_s) is the weight of the hydrogel at time t, and (M_0) is weight of the hydrogel immediately after fabrication, i.e., time 0. The (M_s) was calculated by adding the solid residue weight (M_r) for each hydrogel sample to the recorded weight (M_t) at each time point.

$$M_s = M_t + M_r \qquad \text{(Eq. 2)}$$

To calculate the solid residue weight (M_r), which measures the weight loss due to unreacted prepolymer PEGDA, LAP photoinitiator, and QY photoabsorber leaching out of the crosslinked hydrogels, four samples from both multi-layered (e.g., multi-20 µm and multi-150 µm) and monolithic (e.g., mono-5 mm, mono-3 mm and mono-1.5 mm) hydrogels were fabricated and dried immediately. The average dried weights of the samples ($\overline{M_{d0}}$) was calculated and compared to the dried weight (M_d) of each individual hydrogel, which were stored for 168 hrs at each nominal temperature.

$$M_r = \overline{M_{d0}} - M_d \qquad \text{(Eq. 3)}$$

The change in actual volume of the hydrogel samples was measured using the Normalised Volume Fraction (NVF). It was done by measuring the volume of the hydrogel samples immediately after fabrication (V_i) and every 1.5-2 hrs for 6 hrs and overnight (V_t). The measured volumes were normalised by the initial volume of the hydrogel. The measurements were done by recording the dimensions of the hydrated samples through capturing images, top: Width and length, side: height, using stereo microscope (Zeiss Stemi 305) while they were fully immersed in their water baths [26]. For normalised volume fraction the following formula was used

$$NVF = V_t/V_i \qquad \text{(Eq. 4)}$$

The normalised volume fraction percentage change (ΔNVF) represents the volume change after 24 hrs storage of PEGDA hydrogels at temperatures of 8, 20, 37 and 45 °C. The ΔNVF was calculated using the formula below

$$\Delta NVF = (NVF_t - 1) * 100\% \qquad \text{(Eq. 5)}$$

where (NVF_t) is the normalised volume fraction after 24 hrs.

The reversible thermal response of the multi-layered PEGDA hydrogel to temperature variation was investigated by monitoring the NWF of 4 freshly fabricated multi-layered samples by moving them around 3 water baths with temperatures set at (8, 20, and 45 °C), every 24 hrs for 168 hrs.

2.4 Scanning Electron microscopy (SEM)

The interlayers of the multi-layered PEGDA hydrogel were imaged using SEM (VEGA3, TESCAN) at an acceleration voltage of 10 kV and 3 nA beam current. The hydrogel samples were prepared using freeze-drying method to remove water. The samples were coated with 20 nm gold using sputter coater.

3. Results

The ^{1}H NMR spectrum of PEGDA prepolymer solution showed two peaks at 3.8 ppm, which are attributed to the PEGDA oligomers, and 3 set of peaks centred at 6.25 ppm, which are attributed to the CH_2=CH- double bonds (Figure. 3). The peaks associated to aromatic protons from the LAP photoinitiator and QY photoabsorber are observed between 6.90 and 8.20 ppm (Figure. 3). Two peaks at 2.00 and 2.25 ppm are attributed to one CH_3 and two CH_3, respectively, of the LAP photoinitiator. The peak at 4.8 ppm is attributed to the solvent Deuterium hydrogen monoxide (HOD).

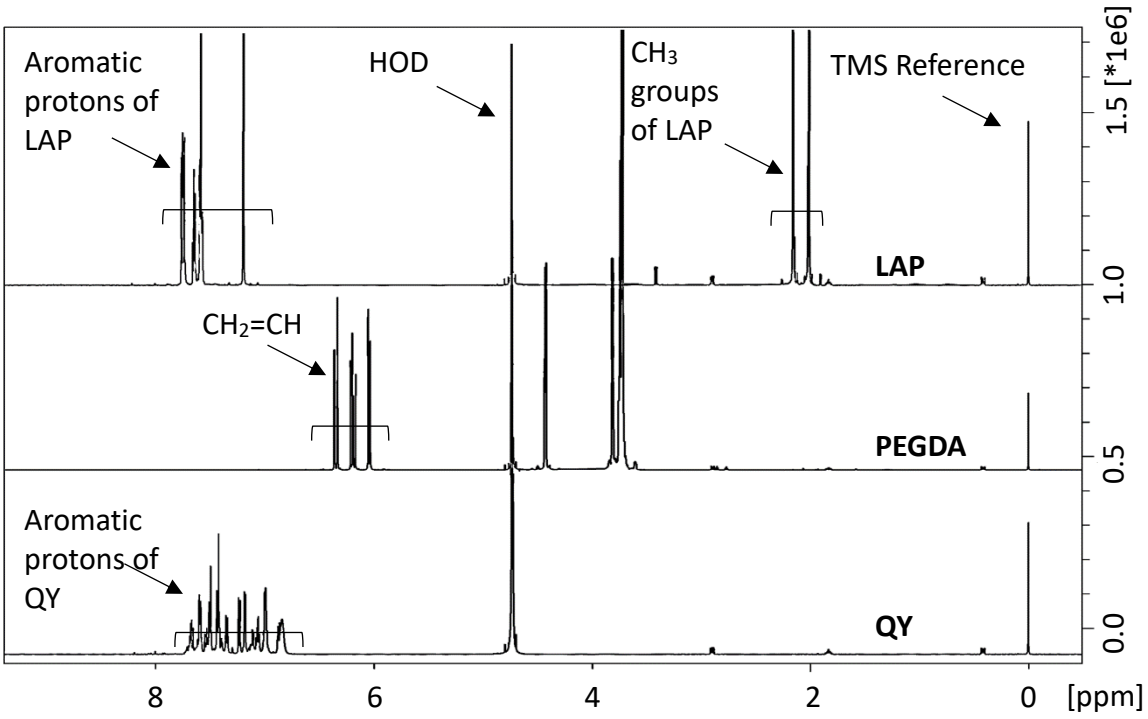

Figure 3: ^{1}H NMR spectra of the PEGDA hydrogels starting materials in D_2O. LAP photoinitiator (top) exhibits peaks of CH_3 groups at 2 and 2.25 ppm and aromatic protons between 6.9 and 8.20 ppm. PEGDA monomer (middle) exhibits peaks of the CH_2=CH- double bonds centred at 6.25 ppm. QY photoabsorber (bottom) exhibits peaks of aromatic protons between 6.9 and 8.2 ppm. The peak at 0 ppm is attributed to TMS reference.

The ^{1}H NMR spectrum of the D_2O solution, in which mono-5 mm hydrogel had been stored for 24 hrs, exhibits negligible peaks at 6.25 ppm that can be attributed to the CH_2=CH- double bonds of PEGDA. As only traces of a soluble PEGDA oligomeric fraction can be observed as two peaks centred at 3.8 ppm, this suggests that the fabrication of mono-5 mm hydrogel yields an almost 100% crosslinking of the PEGDA prepolymer into PEGDA polymer (Figure 4). Conversely, the ^{1}H NMR spectra of the D_2O solutions after 24 hrs of storage from

the multi-20 µm and multi-150 µm hydrogels were observed to exhibit peaks attributed to CH_2=CH- double bonds at 6.25 ppm. This suggests that a small fraction of PEGDA prepolymer was trapped in multi-layered hydrogels during the photo-crosslinking process. Repeat measurements on multi-20 µm hydrogels confirmed a similar degree of crosslinking of PEGDA polymer and reproducibility of the crosslinking data. The thermal analysis of the dry multi-20 µm, multi-150 µm, and mono-5 mm PEGDA hydrogel revealed the glass transition temperatures of the all the PEGDA polymers were between -41 °C and -43 °C using DSC (SI, Figure S1a). On the other hand, the glass transition temperature of the prepolymer PEGDA solution was -15.4 °C (SI, Figure S1b). These findings confirm that crosslinking process has taken place during the photo-crosslinking process.

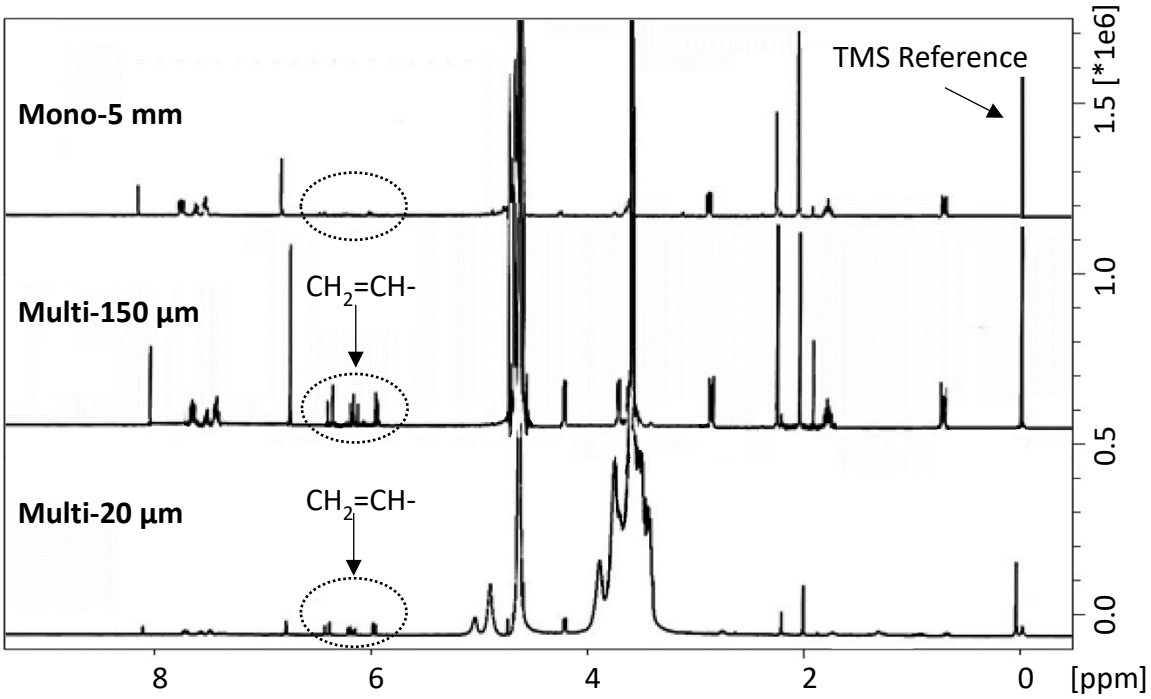

Figure 4: ^{1}H NMR spectra of the solid residue after 24 hrs storage in D_2O from the PEGDA hydrogels: mono-5 mm (top), multi-20 µm (middle), and multi-150 µm (bottom) in D_2O. The

peak at 0 ppm is attributed to TMS reference. Major peaks of CH_2=CH double bonds of PEGDA are at 6.25 ppm, CH_3 groups from LAP at 2 and 2.25 ppm, and aromatics protons of QY and LAP between 6.9 and 8.2 ppm.

Note that the amount of solid residue leaching out of the hydrogels into the storing media was observed to be dependent on the storage temperature. The mass of the solid residue within 168 hrs of storage in DI water was observed to be up to 7 mg on average, which is up to 4.4% of the original weight after fabrication. This was calculated through use of normalised dried weight (NDW) (SI, Eq.S5) for multi-20 µm and multi-150 µm and mono-5 mm hydrogels which were stored at the nominal temperatures of 8, 20, 37 and 45 °C (SI, Figure S3). Higher storage temperatures resulted in the release of higher mass, where the temperatures of 8 °C and 45 °C yield mass release of about 3.5% and 8%, respectively (SI, Figure S3).

The weight of multi- 150 µm hydrogels reduced rapidly within the first 4.5 hrs, as indicated by a decrease in NWF (Eq. 1) to 0.96 and 0.90 when the temperature was raised to 37 °C and 45 °C, respectively, from the fabrication temperature of about 20°C. In contrast, NWF of multi- 20 µm hydrogels was surprisingly increased at 45 °C and 37 °C to 1.01 and 1.04 in the first 4-6 hrs, but then it dropped slightly to 0.95 and 1 after 24 hrs, respectively (Figure 5a). For both multi-20 µm and multi-150 µm, the NWF at a lower temperature of 8 °C increased to 1.14 and 1.24 in the first 4.5 hrs and remained relatively constant there after (Figure 5a). All multi-20 µm, multi-150 µm and mono-5 mm PEGDA hydrogels reached constant mass at around 6 hrs of being stored in the temperature-controlled water baths

at 8, 20, 37 and 45 °C. For mono-5 mm hydrogels, similar pattern with lower NWF values were recorded (Figure 5a). However, monolithic hydrogels appeared to be more thermal sensitive towards elevated temperatures of 37 °C and 45 °C. Note that NWF is a measure of weight fraction in the sample due to water uptake and release at different time points, which is at unity at 0 hr for all multi-layered and monolithic hydrogel samples.

A similar behaviour was observed when the thermal response was quantified volumetrically (Figure 5b). The NVF in multi-20 µm hydrogels stored at 8 °C was slightly higher than that of the multi-150 µm hydrogels. In the first 2 hrs, the NVF in multi-20 µm increased to 1.11, while that of multi-150 µm increased to 1.07. Although mono-5 mm PEGDA hydrogels had a similar overall behaviour to the multi-20 µm and multi-150 µm ones, the magnitude of volume fraction for samples stored at 37 and 45 °C exceeded that of multi-20 µm and multi-150 µm hydrogels. In the first 4 hrs, the volume of mono-5 mm samples increased at 37 and 45 °C to reach NVF of 0.86 and 0.84, respectively, while that of multi-20 µm and multi-150 µm samples was found at 0.93 and 0.91, respectively (Figure 5b). The dimensional change due to the temperature variation at nominal storage temperatures of 45, 37, 20 and 8 °C for multi-150 µm hydrogels can be visually observed (Figure 6a). Note that these hydrogels were fabricated at a temperature of 20°C and this visual observation was carried out 168 hrs after fabrication.

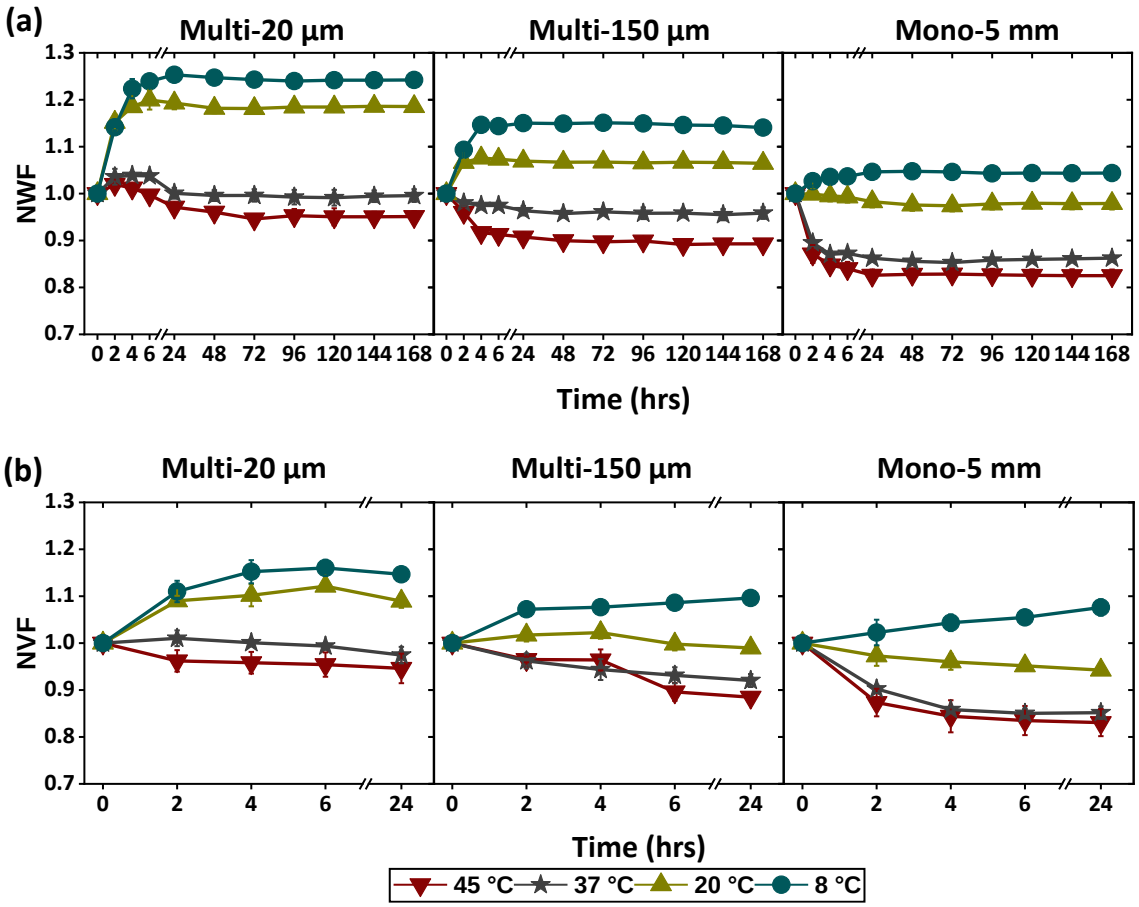

Figure 5: (a) NWF of multi-20 µm and multi-150 µm and mono-5 mm PEGDA hydrogels for up to 168 hrs after fabrication, which is denoted herein as the 0 hrs. **(b)** NVF of multi-20 µm and multi-150 µm and mono-5 mm PEGDA hydrogels samples within 24 hrs of the initial fabricated state. Error bars represent standard deviation from the mean, with n= 4 and n= 3 for independent multi-layered and monolithic samples, respectively. Some error bars are not visible as they are smaller than the data point symbols. All lines are guide to the eye only.

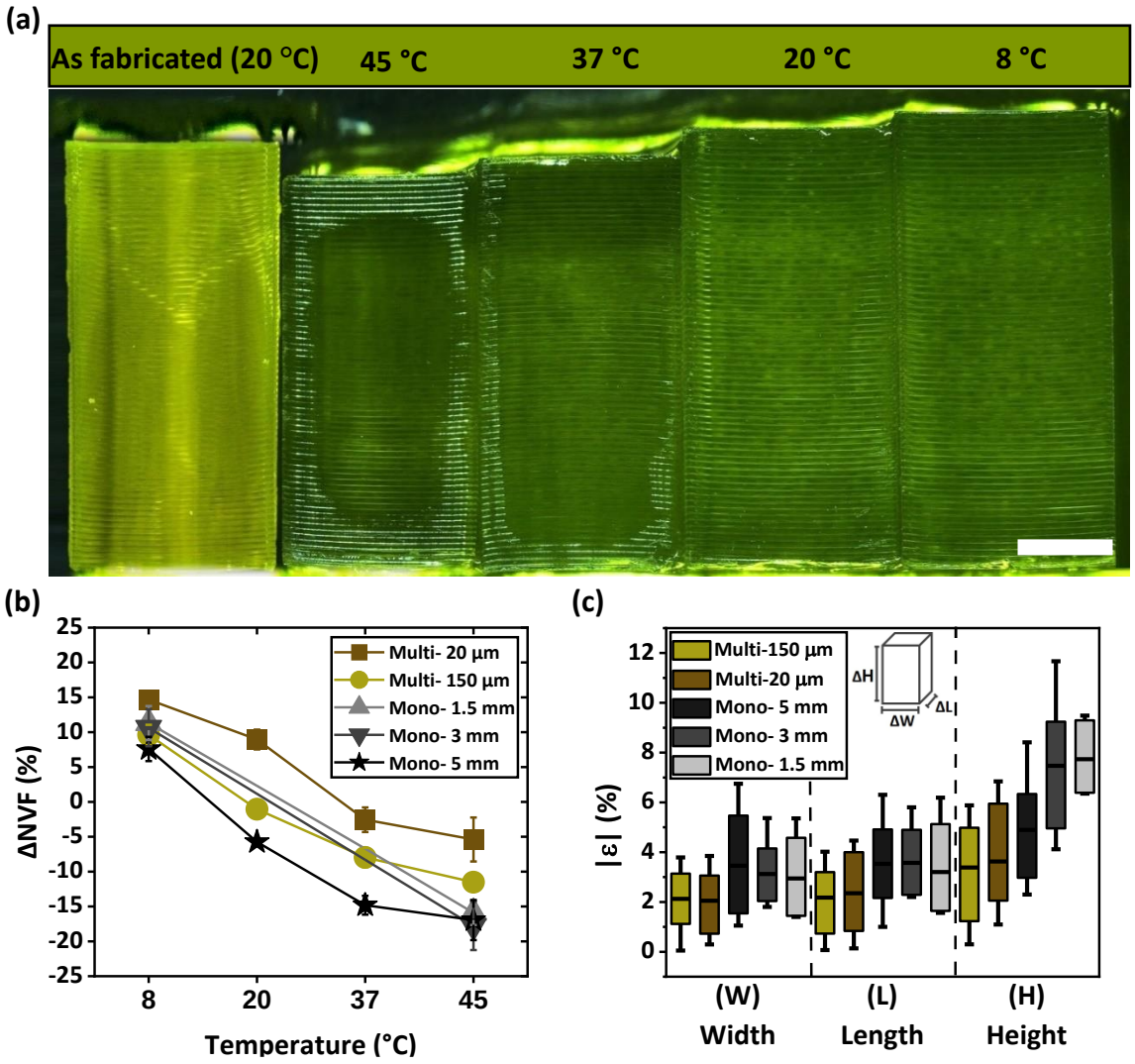

Figure 6: (a) Microscopy image of the multi-150 µm hydrogels (composed of total of 67 layers) as fabricated and 168 hrs after fabrication where samples were stored at nominal temperatures of 45, 37, 20 and 8 °C. Image scale bar is 5 mm. **(b)** Comparison of the change in NVF (ΔNVF) for both multi- 20 µm and multi-150 µm and mono-5 mm, mono-3 mm and mono-1.5 mm hydrogel samples 24 hrs after fabrication. Error bars represent standard deviation from the mean n= 4 and n= 3 for multi-layered and monolithic independent samples, respectively. Some error bars are not visible as they are smaller than the data point

symbols. All lines are guide to the eye only. **(c)** Lateral and axial strain (|ε|) (SI, Eq.S 2-4) in both multi- 20 µm and multi-150 µm and mono-5 mm, mono-3 mm and mono-1.5 mm hydrogel samples 24 hrs after fabrication. The whiskers represent the 1.5 times interquartile range. The median for each data set is identified by a horizontal line and the outliers are shown as diamond symbols.

ΔNVF (Eq. 5) is observed to be monotonically decreasing as temperature increases with a similar rate for all samples within the first 24 hrs after fabrication (Figure 6b). The thinner hydrogel samples exhibit a more positive ΔNVF than the thicker ones. For instance, for multi-layered hydrogels, the multi-20 µm hydrogels had a higher ΔNVF than that of multi-150 µm at all temperature. The ΔNVF for multi-20 µm at temperatures of 8 °C and 45 °C was observed to be +15% and -5%, respectively, compared to +10% and -12%, respectively, for the multi-150 µm hydrogels (Figure 6b). A similar behaviour was observed with monolithic samples, where the ΔNVF of the mono-1.5 mm was higher than that of the mono-5 mm at temperatures of 8 °C and 45 °C (Figure 6b).

The change in volume itself was found to be asymmetric for all samples, where the strain in the axial direction, i.e. height, was considerably higher at approximately 58% on average compared to the lateral change, i.e. width and length (Figure 6c). The magnitude of lateral ($|\varepsilon_W|$ and $|\varepsilon_L|$) and axial strains ($|\varepsilon_H|$) was calculated by equations (SI, Eq.S 2-4). This was done by calculating the dimensions change for width, length, and height for each sample within the first 24 hrs. Note that the axial direction of the samples is defined as the direction at which the UV light was applied onto the samples and the lateral direction is the plane of

the sample normal to the direction of the UV light. It was observed that the thinner hydrogel samples, both multi-layered and monolithic, exhibited slightly lower $|\varepsilon_W|$ and $|\varepsilon_L|$ but higher $|\varepsilon_H|$ than the thicker ones (Figure 6c). For multi-layered samples, $|\varepsilon_H|$ of multi-20 µm was observed to be up to 5% higher than that of multi-150 µm hydrogels. Similarly for monolithic samples, $|\varepsilon_H|$ of mono-1.5 mm is up to 53.8% higher than that of mono-5 mm hydrogels.

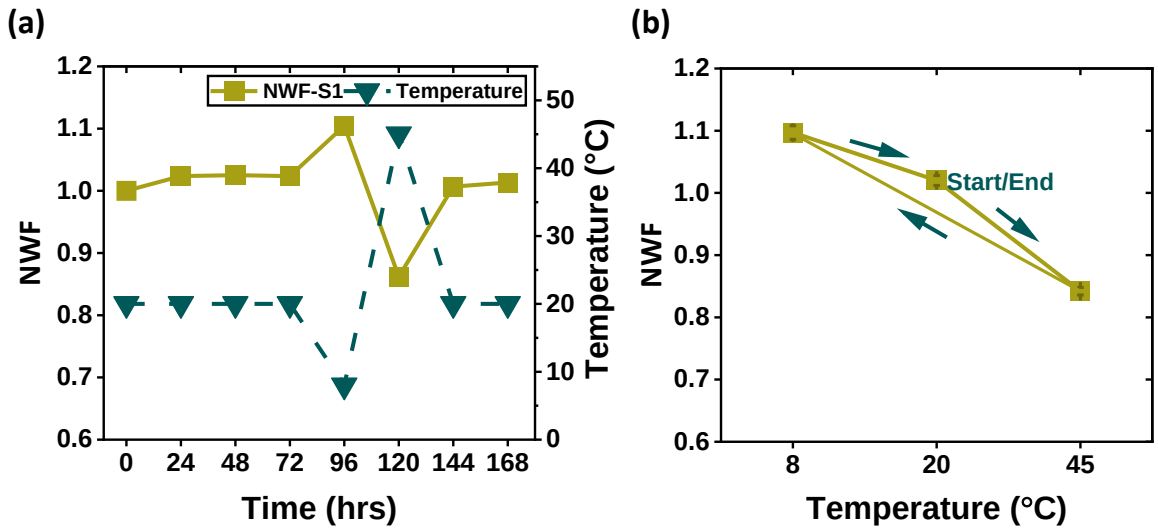

Figure 7: Thermal response of individual multi-150 µm hydrogels to temperature variation for 168 hrs. **(a)** NWF of a multi-150 µm hydrogel moved between different water baths at 8, 20 and 45 °C as set times. **(b)** Average NWF of 4 independent multi-150 µm hydrogels stored and moved in between different water baths. Arrows in (b) represent pattern of temperature change in different water baths. Error bars represent standard deviation from the mean n= 4 for (b). Some error bars are not visible as they are smaller than the data point symbols. All lines are guide to the eye only.

The thermal response of PEGDA hydrogels was observed to be fully reversible within the temperature range of 8–45°C (Figure 7a). For a multi-150 µm hydrogel, the NWF reached 1.02 while being stored at 20 °C for 24 hrs after fabrication. The NWF of the same sample increased to 1.10 when the temperature was decreased to 8 °C. The NWF dropped to 0.85 when the temperature was increased to 45 °C within 24 hrs of storage, which then increased back to 1.02 when subsequently stored at 20 °C for the following 24 hrs of storage. This strongly suggests that the inversed correlation behaviour between NWF of PEGDA hydrogels and storage temperature, in which NWF monotonically decreases with the increase of temperature, can be fully reversed (Figure 7b).

4. Discussion

This work demonstrated the feasibility of manufacturing multi-layered PEGDA hydrogels using projection lithography technique and QY as photoabsorber with a nominal thickness of 20 and 150 µm. QY was utilised to limit the UV light penetration into the prepolymer solution [18], thus a control over the thickness of the crosslinked layer could be enabled by controlling its concentration. With concentration of 1.8 and 9 mg/mL QY, at UV light dosage of 120 mJ/cm2, the crosslinking depth was calculated using optical microscope to 299 ± 5 µm and 46 ± 2 µm (SI, Figure S5 and S6). The nominal layer thickness was set to be approximately half that of the crosslinking depth at 20 µm and 150 µm for multi-20 µm and multi-150 µm. Therefore, each layer was inevitably exposed twice to the UV light as the structure was built top down. It was suggested that the double exposure may enhance bonding between neighbouring layers [18]. NMR spectra showed that the average degree

of crosslinking across the structure in multi-20 µm and multi-150 µm and mono-5 mm PEGDA hydrogels were different. The mono-5 mm, which did not contain QY photoabsorber in its prepolymer solution, had the highest degree of crosslinking, while multi-20 µm with the highest QY concentration had the lowest crosslinking. This suggests that a higher QY photoabsorber concentration in the prepolymer solution leads to a lower degree of crosslinking in the resulting polymer. Caution must be taken to avoid overexposure, which may be detrimental to the mechanical properties required for cardiomyocyte studies due to increased crosslinking density which may lead to stiffer hydrogels [18,27–29]. As the mechanical properties of PEGDA are dependent on the degree of crosslinking, this creates an opportunity to tailor the properties of the photo-crosslinked structures by tuning the fabrication parameters, e.g. UV light dosage, QY photoabsorber concentration and number of layers. These parameters, and thus the properties, can then be optimised to meet the requirement of specific applications [30]. For instance, soft hydrogels for use in cardiac tissue development can be fabricated by high QY photoabsorber concentration and number of layers and low UV dosage [31].

Based on the significance of the slope of the regression lines for all nominal temperatures of 8, 20, 37 and 45 °C, it was found that multi-layered PEGDA hydrogels stored at 37 °C and 45 °C reached equilibrium after 24 and 72 hrs, respectively. In contrast, PEGDA hydrogels stored at 8 °C reached equilibrium after 1.5 hrs and those stored at 20 °C reached equilibrium in less than an hour after fabrication. The monolithic PEGDA hydrogels had different behaviours, where the equilibrium was reached between 4-6 hrs for all

temperatures (Figure 5.a). This suggests that the onset of mass equilibrium for both multi-layered and monolithic PEGDA hydrogels can be reached after 24 hrs at temperatures of 8, 20, and 37 °C, which is comparable to previous study on 3D printed PEGDA composite hydrogels [27]. In contrast, it took 72 hrs to reach equilibrium for temperature of 45°C. PEGDA hydrogels are at equilibrium when the rate of water expulsion slows down, as the osmotic pressure inside and outside the polymeric network reaches similar levels [26]. The variation in the EWC of multi-20 µm and multi-150 µm and mono-5 mm hydrogels can be attributed to the variations in concentration of the PEGDA monomer in the prepolymer solution prior to the photo-crosslinking process (SI, Figure S2). Changes in the concentration of PEGDA monomer in the prepolymer solution has been observed to directly influence the swelling kinetics of the crosslinked hydrogel [32].

While the NVF measurements were showing similar thermal response behaviour to NWF, it was suggested that this is not fully proportional to the gravimetric behaviour [26]. We observed that after 24 hrs, both multi-20 µm and multi-150 µm and mono-5 mm PEGDA hydrogels did not reach volumetric equilibrium. The network polymer chain itself may take much longer period of time to rearrange itself and dimensionally stabilise. It has been reported that some hydrogels, e.g. poly(N-isopropylacrylamide) PNIPAAm, require more than a month to reach volumetric equilibrium [33]. Since the volumetric observations were only taken every 2 hrs for 6 hrs and at 24 hr after fabrication, there were not enough data for a thorough and statistically reliable equilibrium hypothesis testing based on slope of the regression line. Therefore, it is inconclusive to suggest if PEGDA hydrogels have reached

volumetric equilibrium within 24 hrs. For applications where dimensional stability of the crosslinked hydrogel is essential, e.g. for *in vivo* and *in vitro* tissue studies, the fabricated hydrogels may need to be prestored at constant 37 °C for more than 24 hrs before proceeding with experimentation.

The difference in ΔNVF between the multi-layered and monolithic hydrogels may be attributed to variations in the degree of crosslinking in the fabricated PEGDA hydrogels. The higher degree of crosslinking leads to a higher volumetric percentage change in the monolithic hydrogels compared with multi-layered hydrogels. The fact that the volume changes but mass remains the same suggests that the density of the hydrogel is not constant before reaching volumetric equilibrium. This is vital for the calculation of theoretical mesh size or porosity, as it is typically assumed that the polymer density is constant.

It is important to note that the strain in the axial direction ($|\varepsilon_H|$) was considerably higher than that of the lateral ($|\varepsilon_W|$) and ($|\varepsilon_L|$) for both multi-layered and monolithic PEGDA hydrogels (Figure 6c). The anisotropic characteristic can be attributed to the formation of highly crosslinked planer sublayers at the interface of each layer. We hypothesise that these planar sublayers are thermally and structurally more stable than the remaining part of each layer. This leads to the formation of an isostrain condition in lateral direction and an isostress condition in the axial direction. When the fabricated hydrogels undergo thermally induced volumetric strain, the highly crosslinked planar sublayers are able to limit the strain in the isostrain condition better than in the isostress condition. Therefore, the strain in the

lateral direction is expected to be much less than that in the axial direction. This is in agreement with our observation where the swelling and shrinkage are higher in the axial direction rather than in the lateral direction (Figure 6c). Further observation on the figure (Figure 6c), suggest that the multi-20 µm hydrogels have higher axial dimensional change compared with the multi-150 µm. This further supports our hypothesis that a larger portion of the highly crosslinked planar sublayers within the hydrogel structure leads to a more stable structure along the direction of the sublayers, i.e. lateral direction, while maintaining compliance in the direction normal to the sublayers, i.e. axial direction. SEM images of the multi-layered hydrogel confirm the presence of highly crosslinked planar sublayer at the first surface of each layer (Figure 8).

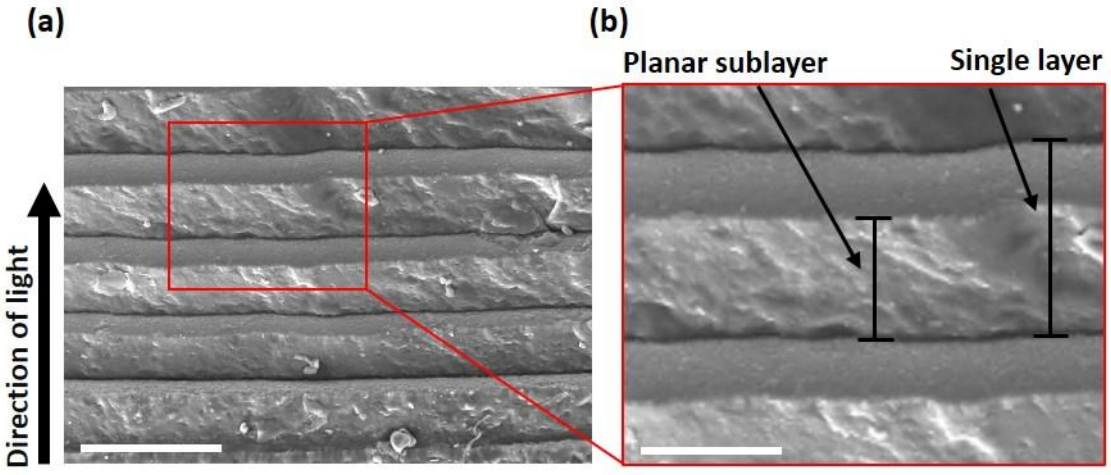

Figure 8: SEM image of a freeze dried multi-150 µm PEGDA hydrogel showing the highly crosslinked planar sublayers at the first surface of each layer. Scale bar for (a) and (b) are 200 µm and 100 µm, respectively.

A similar behaviour is also observed on the monolithic samples. The strain of three monolithic hydrogels, i.e. mono-5 mm, mono-3 mm and mono-1.5 mm, show that shorter structures correspond to higher $|\varepsilon_H|$ (Figure 6c). This suggest that the degree of crosslinking varies across the heights of monolithic samples in a similar fashion to the multi-layered samples. Such a variation can be attributed to the crosslinking depth of the UV irradiation at a wavelength of 365 nm and a dosage of 120 mJ/cm^2 into the PEGDA hydrogels.

Note that the thermal response of all three monolithic hydrogels exhibits similar expansion and shrinkage behaviours to each other, as indicated by the similarity of their ECW, NWF, and NVF (SI, Figure S4). This finding contradicts earlier findings where the UV photo-crosslinked PEGDA hydrogels with no photoabsorber were classed as isotropic gels [34]. For a collimated or slightly diverging UV irradiation source, the highly crosslinked sublayer is planar and normal to the direction of the impinging UV light. Therefore, PEGDA hydrogels manufactured by projection lithography are expected to be anisotropic due to the presence of these sublayers. This anisotropy may be reduced by maximising the portion of the highly crosslinked sublayers within the hydrogels by post fabrication multiaxial UV exposure. Further investigation is needed to fully elucidate the underlying mechanism governing this anisotropy behaviour.

Our gravimetric and volumetric analysis suggests that the thermal response of PEGDA hydrogels can be attributed to changes in hydrogen bonds strength at different temperatures. PEDGA comprises of hydrophilic (O-CH2-CH2) repeating unit backbone called oxyethylene compound [35] and acrylates side chains containing hydroneutral vinyl groups

[36]. The oxyethylene chain interacts favourably with the low temperature water structures and less favourably with the high temperature forms of water [37], as its average conformation changes from being more polar at low temperatures to being less polar at high temperatures [38]. At fabrication temperature of about 20°C, the backbone oxyethylene chain absorbs water molecules until it reaches equilibrium. With increased temperatures the oxyethylene chain undergoes drastic change from hydrophilic to hydrophobic because the negative entropy of water molecules around the nonpolar regions of PEGDA dominates [39]. Even though the hydrogel multi-layered PEGDA hydrogels are fully immersed in water, the hydrogen bonds are weakened and water molecules are desorbed and expelled from the polymer chain due to the dominant hydrophobic interactions between backbone groups at an elevated temperature [40,41]. The desorption of the water molecules results in shrinkage in the PEGDA polymer network (Figure 9). In addition, the outside region of the membrane would be affected first and thus the hydrophobic interactions among the vinyl groups in the outer regions become stronger. This leads to the rapid shrinkage of the outermost surface, forming a dense skin layer that prevents the free water from diffusing out and thus prolonging the response rate [40,42,43]. The opposite behaviour was also observed, where the increased polarity in lower temperatures results in stronger hydrogen bonds between the water molecules and the polymer network, hence more absorption of water molecules into the polymer network and higher swelling [44–46].

As multi-layered PEGDA hydrogels respond reversibly to temperature changes and undergo reversible phase transition [44], they can be potentially used in a range of temperatures without suffering from thermal degradation by repeated temperature changes. A thermal responsive PEGDA hydrogel exhibits a reversible expansion/shrinkage transition where the polymer can revert back to its original state of equilibrium, within a certain temperature range, above or below the critical gel transition temperature (CGTT) [41]. It has been reported that PEGDA with molecular weight of 400 had a CGTT between 34-36 °C [45]. Even though it was not investigated herein, we can speculate that the CGTT of our polymer would have similar values to that of PEGDA 400. This suggests that the mass lost/gained through the thermal expansion/shrinkage process may be recuperated within the 24 hrs period if the storage temperature goes above or below 34-36 °C.

All the aforementioned findings suggest that PEGDA is a macroporous hydrogel that absorbs water molecules into its pores. The water absorption behaviour is strongly dependent on temperatures, as it is influenced by the contributions of free water, non-bound water, (NBW), weakly bound water (WBW), and strongly bound water (SBW) (Figure 9) [47]. The main portion of water is attributable to free water and NBW located within macropores. As the temperature increases above the fabrication temperature (T_0), polymeric chains start to aggregate, phase separation takes place and the shrunk micropores expel the free water, NBW and WBW from the PEGDA polymer network [33,48]. The SBW which forms the primary hydration shell around the PEGDA polymer chains that is located within the micro and nanopores in the macropore walls is not effected by range of temperature in the study,

as they are strongly bound to the network chain and are normally trapped within the nanopores [26,47,49]. The size, distribution and alignment of the pores in the hydrogel is of relevance for in vitro studies, as they affect attachment of the living tissues, muscles, and their performance [50].

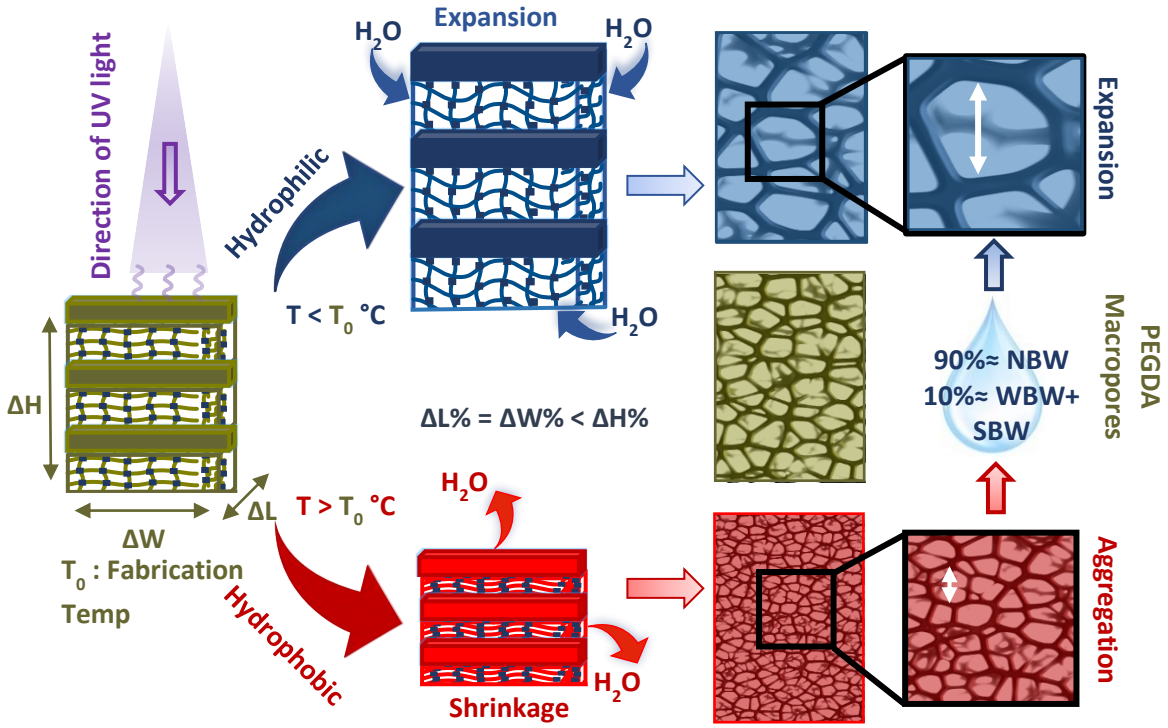

Figure 9: Schematic of anisotropic thermoresponsive behaviour of PEGDA hydrogels, where above and below fabrication temperature, an unequal (ΔL% = ΔW% (lateral) < ΔH% (axial)) volume change is observed. Below fabrication temperature, due to higher NBW absorption and stretching of macropores, there is a volume expansion. Above fabrication temperatures, the NBW and WBW are expelled from the network, macropores aggregate and hydrogel shrinks.

5. Conclusions

This study was directed to investigate the thermal response of multi-layered and monolithic photo crosslinked PEGDA hydrogels. The equilibrium weight and volume of photo crosslinked PEGDA hydrogels at storage temperatures of 8–45°C was observed to change between +14% and -19%. At 37 °C, which represents the incubation temperature, a negative 5–15% weight and volume change was observed. The Normalised Volume Fraction (NWF) of the multi-20 μm and multi-150 μm hydrogels increased to +14% at lower 8 °C temperature, whereas the NWF decreased to -11.1% at 45 °C. As a result of the water uptake and release, the volume of the PEGDA hydrogels also changed. The NVF results showed that the multi-20 μm and multi-150 μm layered hydrogels experienced expansion of approximately +10% at 8 °C, while they shrunk at 45 °C to -11.5%. This expansion and shrinkage were observed to be due to change in the oxyethylene chain of the polymer network when temperature changes. The backbone of the PEGDA polymer network undergoes drastic change from hydrophilic to hydrophobic at elevated temperatures. This weakens the hydrogen bonds and water molecules are expelled from the polymer chains due to the dominant hydrophobic interactions between backbone groups. The desorption of the water molecules results in shrinkage in the PEGDA polymer network. At lower temperatures, an opposite behaviour was seen, where stronger hydrogen bonds between the water molecules and the polymer network due to increased polarity, results in more absorption of water molecules into the polymer network and higher polymer expansion.

These findings suggests that differences in the degree of polymerisation and application temperatures have to be considered in the design and fabrication process. In addition, the

observed anisotropic behaviour of photo crosslinked PEGDA hydrogel between the axial and lateral directions must be taken into account into the design of the UV irradiation direction during the polymerisation process. A projection lithography of PEGDA hydrogels using a single UV irradiation source leads to a large anisotropic characteristic, where the thermal responses in axial dimension was about 58% higher than those in lateral dimension. The multi-layered PEGDA hydrogels were observed to have reversibility behaviour at temperatures of 8–45°C. However, further investigation with high number of cycles or frequency needs to be undertaken to fully understand the effect of the temperature cycles on the degradation of the hydrogels. The findings presented herein should be considered as a basis for further studies into the effect of fabrication protocol and environmental conditions on the long term physicochemical and thermomechanical behaviour of the PEGDA hydrogels, which are crucial to many future biomedical and bioengineering applications.

Supplementary Information:

The data that support the findings of this study are openly available in CORD at http://doi:10.17862/cranfield.rd.15169203.

Supplementary material includes, Tg, EWC calculation, NDW, and equations required to calculate the magnitude dimensional change and EWC, NWF and NVF of mono-5, 3 and 1.5 mm hydrogels.

Declaration of Competing Interest:

The authors declare that they have no known competing financial interests or personal relationships that could have appeared to influence the work reported in this paper.

Author contributions

Mohammad Hakim Khalili: Formal analysis, Investigation, Writing- Original draft, Visualisation, Conceptualisation. **Ashfaq Afsar:** Formal Analysis, Investigation, writing- Original draft. **Rujing Zhang:** Writing- review & editing. **Sandra Wilson:** Writing- review & editing. **Eleftheria Dossi:** Writing- review and editing, Formal Analysis, Supervision, Conceptualisation. **Saurav Goel:** Writing- original draft, Supervision, Funding acquisition. **Susan. A Impey:** Writing- original draft, Supervision, Funding acquisition, Conceptualisation. **Adrianus Indrat Aria:** Writing- review & editing - Original draft, Supervision, Funding acquisition, Conceptualisation.

Acknowledgements

All authors greatly acknowledge the financial support provided by the UKRI via Grants No. EP/L016567/1, EP/S013652/1, EP/S036180/1, EP/T001100/1 and EP/T024607/1, TFIN+ Feasibility study award to LSBU (EP/V026402/1), the Royal Academy of Engineering via Grants No. IAPP18-19\295 and TSP1332, EURAMET EMPIR A185 (2018), the EU Cost Action (CA15102, CA18125, CA18224 and CA16235) and the Newton Fellowship award from the Royal Society (NIF\R1\191571). We also thank the Cranfield Forensic Institute for accessing their optical microscopy laboratory funded by SEMLEP through the Local Growth Fund and Cranfield University.

References

1. Koons GL., Diba M., Mikos AG. Materials design for bone-tissue engineering. Nature Reviews Materials. Springer US; 2020; 5(8): 584–603. Available at: DOI:10.1038/s41578-020-0204-2

2. Pryzhkova M V., Aria I., Cheng Q., Harris GM., Zan X., Gharib M., et al. Carbon nanotube-based substrates for modulation of human pluripotent stem cell fate. Biomaterials. Elsevier Ltd; 2014; 35(19): 5098–5109. Available at: DOI:10.1016/j.biomaterials.2014.03.011

3. Cao Y., Yao Y., Li Y., Yang X., Cao Z., Yang G. Tunable keratin hydrogel based on disulfide shuffling strategy for drug delivery and tissue engineering. Journal of Colloid and Interface Science. Elsevier Inc.; 2019; 544: 121–129. Available at: DOI:10.1016/j.jcis.2019.02.049

4. Arabi N., Zamanian A., Rashvand SN., Ghorbani F. The Tunable Porous Structure of Gelatin–Bioglass Nanocomposite Scaffolds for Bone Tissue Engineering Applications: Physicochemical, Mechanical, and In Vitro Properties. Macromolecular Materials and Engineering. 2018; 303(3): 1–12. Available at: DOI:10.1002/mame.201700539

5. Lyon BJ., Aria AI., Gharib M. Fabrication of carbon nanotube—polyimide composite hollow microneedles for transdermal drug delivery. Biomedical Microdevices. 2014; 16(6): 879–886. Available at: DOI:10.1007/s10544-014-9892-y

6. Hansen A., Eder A., Bönstrup M., Flato M., Mewe M., Schaaf S., et al. Development of a drug screening platform based on engineered heart tissue. Circulation Research.

2010; 107(1): 35–44. Available at: DOI:10.1161/CIRCRESAHA.109.211458

7. Vandenburgh H., Shansky J., Benesch-Lee F., Barbata V., Reid J., Thorrez L., et al. Drug-screening platform based on the contractility of tissue-engineered muscle. Muscle and Nerve. 2008; 37(4): 438–447. Available at: DOI:10.1002/mus.20931

8. Cashman TJ., Josowitz R., Johnson B V., Gelb BD., Costa KD. Human engineered cardiac tissues created using induced pluripotent stem cells reveal functional characteristics of BRAF-mediated hypertrophic cardiomyopathy. PLoS ONE. 2016; 11(1): 1–17. Available at: DOI:10.1371/journal.pone.0146697

9. He YJ., Young DA., Mededovic M., Li K., Li C., Tichauer K., et al. Protease-Sensitive Hydrogel Biomaterials with Tunable Modulus and Adhesion Ligand Gradients for 3D Vascular Sprouting. Biomacromolecules. 2018; 19(11): 4168–4181. Available at: DOI:10.1021/acs.biomac.8b00519

10. Chatterjee S., Hui PCL., Kan C wai. Thermoresponsive hydrogels and their biomedical applications: Special insight into their applications in textile based transdermal therapy. Polymers. 2018; 10(5). Available at: DOI:10.3390/polym10050480

11. Choi JR., Yong KW., Choi JY., Cowie AC. Recent advances in photo-crosslinkable hydrogels for biomedical applications. BioTechniques. 2019; 66(1): 40–53. Available at: DOI:10.2144/btn-2018-0083

12. Kumar Thakur V., Kumar Thakur M. Hydrogels. Springer; 2018. 470 p. Available at: DOI:10.1007/978-981-10-6077-9

13. You Y., Xie Y., Jiang Z. Injectable and biocompatible chitosan-alginic acid hydrogels.

Biomedical Materials (Bristol). IOP Publishing; 2019; 14(2). Available at: DOI:10.1088/1748-605X/aaff3d

14. Chan V., Zorlutuna P., Jeong JH., Kong H., Bashir R. Three-dimensional photopatterning of hydrogels using stereolithography for long-term cell encapsulation. Lab on a Chip. 2010; 10(16): 2062–2070. Available at: DOI:10.1039/c004285d

15. Xue P., Zhang X., Chuah YJ., Wu Y., Kang Y. Flexible PEGDA-based microneedle patches with detachable PVP-CD arrowheads for transdermal drug delivery. RSC Advances. Royal Society of Chemistry; 2015; 5(92): 75204–75209. Available at: DOI:10.1039/c5ra09329e

16. Rekowska N., Arbeiter D., Brietzke A., Konasch J., Riess A., Mau R., et al. Biocompatibility and thermodynamic properties of PEGDA and two of its copolymer. Proceedings of the Annual International Conference of the IEEE Engineering in Medicine and Biology Society, EMBS. IEEE; 2019; : 1093–1096. Available at: DOI:10.1109/EMBC.2019.8857503

17. Christensen RK., Von Halling Laier C., Kiziltay A., Wilson S., Larsen NB. 3D Printed Hydrogel Multiassay Platforms for Robust Generation of Engineered Contractile Tissues. Biomacromolecules. 2019; : 1–10. Available at: DOI:10.1021/acs.biomac.9b01274

18. Zhang R., Larsen NB. Stereolithographic hydrogel printing of 3D culture chips with biofunctionalized complex 3D perfusion networks. Lab on a Chip. Royal Society of

Chemistry; 2017; 17(24): 4273–4282. Available at: DOI:10.1039/c7lc00926g

19. Hahn MS., Miller JS., West JL. Three-dimensional biochemical and biomechanical patterning of hydrogels for guiding cell behavior. Advanced Materials. 2006; 18(20): 2679–2684. Available at: DOI:10.1002/adma.200600647

20. Lind M. Technical University of Denmark Micromachined 2D Transducers and Phantoms for 3D Super-Resolution Ultrasound Imaging. 2020;

21. Liu VA., Bhatia SN. Three-dimensional photopatterning of hydrogels containing living cells. Biomedical Microdevices. 2002; 4(4): 257–266. Available at: DOI:10.1023/A:1020932105236

22. Stillman Z., Jarai BM., Raman N., Patel P., Fromen CA. Degradation profiles of poly(ethylene glycol) diacrylate (PEGDA)-based hydrogel nanoparticles. Polymer Chemistry. Royal Society of Chemistry; 2020; 11: 568–580. Available at: DOI:10.1039/c9py01206k

23. Huang H., Qi X., Chen Y., Wu Z. Thermo-sensitive hydrogels for delivering biotherapeutic molecules: A review. Saudi Pharmaceutical Journal. King Saud University; 2019; 27(7): 990–999. Available at: DOI:10.1016/j.jsps.2019.08.001

24. Ionov L. Hydrogel-based actuators: Possibilities and limitations. Materials Today. Elsevier Ltd.; 2014; 17(10): 494–503. Available at: DOI:10.1016/j.mattod.2014.07.002

25. Tsang VL., Chen AA., Cho LM., Jadin KD., Sah RL., DeLong S., et al. Fabrication of 3D hepatic tissues by additive photopatterning of cellular hydrogels. The FASEB Journal.

2007; 21(3): 790–801. Available at: DOI:10.1096/fj.06-7117com

26. Yang X., Dargaville BL., Hutmacher DW. Elucidating the molecular mechanisms for the interaction of water with polyethylene glycol-based hydrogels: Influence of ionic strength and gel network structure. Polymers. 2021; 13(6). Available at: DOI:10.3390/polym13060845

27. Tikhonov A., Evdokimov P., Klimashina E., Tikhonova S., Karpushkin E., Scherbackov I., et al. Stereolithographic fabrication of three-dimensional permeable scaffolds from CaP/PEGDA hydrogel biocomposites for use as bone grafts. Journal of the Mechanical Behavior of Biomedical Materials. Elsevier Ltd; 2020; 110(July): 103922. Available at: DOI:10.1016/j.jmbbm.2020.103922

28. Xue D., Wang Y., Zhang J., Mei D., Wang Y., Chen S. Projection-Based 3D Printing of Cell Patterning Scaffolds with Multiscale Channels. ACS Applied Materials and Interfaces. 2018; 10(23): 19428–19435. Available at: DOI:10.1021/acsami.8b03867

29. Hamid ZAA., Lim KW. Evaluation of UV-crosslinked Poly(ethylene glycol) Diacrylate/Poly(dimethylsiloxane) Dimethacrylate Hydrogel: Properties for Tissue Engineering Application. Procedia Chemistry. Elsevier Ltd.; 2016; 19: 410–418. Available at: DOI:10.1016/j.proche.2016.03.032

30. Körner A., Mosqueira M., Hecker M., Ullrich ND. Substrate Stiffness Influences Structural and Functional Remodeling in Induced Pluripotent Stem Cell-Derived Cardiomyocytes. Frontiers in Physiology. 2021; 12(August). Available at: DOI:10.3389/fphys.2021.710619

31. Zamprogno P., Thoma G., Cencen V., Ferrari D., Putz B., Michler J., et al. Mechanical properties of soft biological membranes for organ-on-a-chip assessed by bulge test and AFM. ACS Biomaterials Science and Engineering. 2021; 7(7): 2990–2997. Available at: DOI:10.1021/acsbiomaterials.0c00515

32. Browning MB., Cosgriff-hernandez E. Development of a Biostable Replacement for PEGDA Hydrogels. Bio MacromoleculesMacromolecules. 2012; 13: 779–786. Available at: DOI:10.1021/bm201707z

33. Chung T., Han IK., Han J., Ahn K., Kim YS. Fast and large shrinking of thermoresponsive hydrogels with phase-separated structures. Gels. 2021; 7(1): 1–10. Available at: DOI:10.3390/GELS7010018

34. Cappello J., d'Herbemont V., Lindner A., Roure O du. Microfluidic in-situ measurement of poisson's ratio of hydrogels. Micromachines. 2020; 11(3): 1–12. Available at: DOI:10.3390/mi11030318

35. De Giglio E., Cometa S., Satriano C., Sabbatini L., Zambonin PG. Electrosynthesis of hydrogel films on metal substrates for the development of coatings with tunable drug delivery performances. Journal of Biomedical Materials Research - Part A. 2009; 88(4): 1048–1057. Available at: DOI:10.1002/jbm.a.31908

36. Sagawa N., Shikata T. Are all polar molecules hydrophilic? Hydration numbers of nitro compounds and nitriles in aqueous solution. Physical Chemistry Chemical Physics. 2014; 16(26): 13262–13270. Available at: DOI:10.1039/c4cp01280a

37. Lindman B., Karlström G. Nonionic polymers and surfactants: Temperature

anomalies revisited. Comptes Rendus Chimie. 2009; 12(1–2): 121–128. Available at: DOI:10.1016/j.crci.2008.06.017

38. Viti V., Zampetti P. Dielectric properties of 2-methoxyethanol and 1,2-dimethoxyethane: Comparison with ethylene glycol. Chemical Physics. 1973; 2(2): 233–238. Available at: DOI:10.1016/0301-0104(73)80009-6

39. Matsumoto K., Sakikawa N., Miyata T. Thermo-responsive gels that absorb moisture and ooze water. Nature Communications. Springer US; 2018; 9(1): 1–7. Available at: DOI:10.1038/s41467-018-04810-8

40. Son KH., Lee JW. Synthesis and characterization of poly(ethylene glycol) based thermo-responsive hydrogels for cell sheet engineering. Materials. 2016; 9(10). Available at: DOI:10.3390/ma9100854

41. Lee W-F., Cheng T-S. Studies on Preparation and Properties of Porous Biodegradable Poly(NIPAAm) Hydrogels. Journal of Applied Polymer Science. 2008; 109.

42. Maiti B., Abramov A., Franco L., Puiggalí J., Enshaei H., Alemán C., et al. Thermoresponsive Shape-Memory Hydrogel Actuators Made by Phototriggered Click Chemistry. Advanced Functional Materials. 2020; 30(24). Available at: DOI:10.1002/adfm.202001683

43. Ryo Y., Katsuml U., Yuzo K., Kiyotaka S., Akihiko K., Yasuhisa S., et al. Comb-type grafted hydrogels with rapid de-swelling response to temperature changes. Nature. 1995; 374(March): 240–242.

44. Zhang Q., Weber C., Schubert US., Hoogenboom R. Thermoresponsive polymers with

lower critical solution temperature: From fundamental aspects and measuring techniques to recommended turbidimetry conditions. Materials Horizons. Royal Society of Chemistry; 2017; 4(2): 109–116. Available at: DOI:10.1039/c7mh00016b

45. Wu WX., Huang YC., Lee WF. Effect of poly(ethylene glycol)-derived crosslinkers on the properties of thermosensitive hydrogels. Iranian Polymer Journal (English Edition). Springer Berlin Heidelberg; 2020; 29(8): 679–691. Available at: DOI:10.1007/s13726-020-00831-7

46. Gomes de Menezes FL., de Lima Leite RH., Gomes dos Santos FK., Aria AI., Aroucha EMM. TiO2-enhanced chitosan/cassava starch biofilms for sustainable food packaging. Colloids and Surfaces A: Physicochemical and Engineering Aspects. Elsevier B.V.; 2021; 630(September): 127661. Available at: DOI:10.1016/j.colsurfa.2021.127661

47. Gun'ko V., Savina I., Mikhalovsky S. Properties of Water Bound in Hydrogels. Gels. 2017; 3(4): 37. Available at: DOI:10.3390/gels3040037

48. Gallagher S., Florea L., Fraser KJ., Diamond D. Swelling and shrinking properties of thermo-responsive polymeric ionic liquid hydrogels with embedded linear pNIPAAM. International Journal of Molecular Sciences. 2014; 15(4): 5337–5349. Available at: DOI:10.3390/ijms15045337

49. Savina IN., Gun'Ko VM., Turov V V., Dainiak M., Phillips GJ., Galaev IY., et al. Porous structure and water state in cross-linked polymer and protein cryo-hydrogels. Soft Matter. 2011; 7(9): 4276–4283. Available at: DOI:10.1039/c0sm01304h

50. Bian W., Juhas M., Pfeiler TW., Bursac N. Local tissue geometry determines contractile force generation of engineered muscle networks. Tissue Engineering - Part A. 2012; 18(9–10): 957–967. Available at: DOI:10.1089/ten.tea.2011.0313